Proceedings of the Fortieth National Conference on Fluid Mechanics and Fluid Power

December 12–14, 2013, NIT Hamirpur, Himachal Pradesh, India

FMFP2013-20

EXPERIMENTAL INVESTIGATION OF WALL SHEAR STRESS DEVELOPED DURING COALESCENCE OF TWO PENDANT DROPS

Praveen M. Somwanshi
Mechanical Engineering
IIT Kanpur 208016
praveens@iitk.ac.in

K. Muralidhar
Mechanical Engineering
IIT Kanpur 208016
kmurli@iitk.ac.in

Sameer Khandekar
Mechanical Engineering
IIT Kanpur 208016
samkhan@iitk.ac.in

Keywords: Pendant Drops, Coalescence, Contact Line, Bridge, Imaging, Wall Shear Stress

ABSTRACT

Coalescence of drops and bubbles are encountered in many engineering applications. In liquids, it is the process by which two or more droplets contact each other and merge to form a single daughter droplet. It may occur in a medium that is entirely fluid or on a solid surface. In both instances, coalescence is an intense dynamic process during which the fluid is momentarily set into motion. The present study investigates shear stresses generated on the wall when two pendant drops coalesce. The experiment is initiated by placing two drops adjacent to each other till a liquid bridge is formed, with the drops just touching each other. The negative curvature at the liquid bridge drives coalescence. The contact line moves and the bridge relaxes as flow takes place from a region of higher to lower pressure. The entire process has been imaged by using a high speed camera. Fluid considered is water on a Teflon surface. The image sequence is analyzed to find the instantaneous centre of mass of the drop, which in turn, yields the velocity components. These velocity components are used to find the time-dependent shear stresses at the wall. Results show that large shear stresses are momentarily developed at the wall. For coated surfaces, coalescence may induce leaching, thus lowering its life.

1. INTRODUCTION

Drop coalescence is a process in which two drops merge to form a daughter droplet. It is a very important phenomenon in mixtures, sintering in metallurgy, ink-jet printing and dropwise condensation.

Coalescence of sessile drops on a horizontal substrate was studied by Andrieu et al. (2002), Thoroddsen et al. (2005[a]), Thoroddsen et al. (2005[b]), Thoroddsen et al. (2007), Narhe et al. (2004) and Wu et al. (2004). Andrieu et al. (2002) found that a bridge is formed when two drops come near each other. The bridge has a large curvature which expands quickly because of surface tension. The bridge relaxes exponentially to form an ellipsoid. The process of coalescence happens over a very short interval of time followed by a number of oscillations. Thoroddsen et al. (2005[a]) found that axisymmetry is retained around the coalescence axis but the shapes of two drops are distorted differently by gravity. The ratio of the two principal radii of curvature increases linearly with time. The coalescence motions are reasonably compatible with the power law scaling, $R \propto t^{0.5}$ where R is neck radius and t is time. For the early coalescence the power law coefficient is 0.46 which is slightly

lower than the actual and might be caused by finite initial contact radius. The power law coefficient is 0.41 for larger radii of curvature. Coalescence speed decreases for the drops of higher viscosity whose Reynolds number is less than 5000. Viscous forces affect the coalescence speed if radii of curvature are smaller than 70 μm. The curvature in the neck regions becomes sharper and shape changes qualitatively with increase in viscosity. Thoroddsen et al. (2005[b]) found that the interface shapes include best-fit circular arcs in the neck region. The merging shapes have constant curvature with a sharper positive curvature when the circle meets the initial surface. The center of the circle shifts downwards from the original contact height because of different shapes of the drop. The ratio of two principal radii of curvature increases linearly with time. The linear fit does not extrapolate through zero. There is no secondary reconnection because of poor spatial resolution at the neck radius. Small amplitude capillary waves are observed ahead of the circular neck. Capillary waves produce interface distortions. Thoroddsen et al. (2007) reported that the coalescence speed depends on the lower value of surface tension of the fluids. A thin layer of ethanol is pulled down along the surface of water drop because of the surface tension. Sharp corners are observed at the interface because of the difference in viscosities. The corner becomes sharper for highest difference in viscosities. The radius of curvature is inversely proportional to the dynamic viscosity. The reduced surface tension decreases the speed of coalescence. Self similar shapes are observed when water drop coalesces with a pool of ethanol. The relative strength of the molecular diffusivity of ethanol versus the wave speed changes with drop size. Pinning affects the wave amplitudes. This additional pinning destroys self similarity of the Marangoni waves. The scaling is found to be $R \propto t^{0.5}$ where R is radius of drop and t is time. Flow occurs along the curved surface and generates vortices. Narhe et al. (2004) reported that the composite drop formed due to coalescence relaxes exponentially toward equilibrium. The relaxation time is larger by 5 to 6 orders of magnitude than that predicted by bulk hydrodynamics. Excitation is observed in spreading experiments while it is absent during coalescence. The rate depends on initial kinetic energy given to the drop at the beginning of its relaxation. Syringe deposition induces strong oscillations. The drop surface pulls the contact line at each oscillation which accelerates its motion. Coalescence during condensation has no oscillations thereby decreasing relaxation by a factor of 10-100.The study of contact line motion with traditional drop deposition is not accurate enough because of uncontrollable oscillations. However, within experimental error there is no influence of condensation/evaporation on the contact line motion. *K,* the ratio of shear viscosity to dissipation coefficient was found to be $1O^{-4}$ for the syringe deposition and 2.4×10^{-6} in condensation coalescence. Such small values of *K* show that the dynamics of sessile drop is limited by dissipation at the region of drop close to the contact line. This dissipation leads to relaxation 5 to 6 orders of magnitude slower than the bulk dissipation. Wu et al. (2004) studied the coalescence of sessile drops. The liquid bridge radius follows the scaling law, $r_b \propto t^{0.5}$ where r_b is bridge radius and t is time. The contact line between the drop and the syringe tip is pinned between the receding and advancing contact angles. Capillary waves are seen in water and methanol mixtures while they are absent in water-glycerol mixtures. Early time evolution of the bridgewidth and air-drop interface are similar near the bridge. The dimensional slope is measured to be 1.14-1.33 for two drops of unequal size. The fluid properties have little influence on the dimensionless scaling law pre-factor but modifiy the shape of interface near the liquid bridge. Yeh et al. (2013) studied the coalescence of sessile drops on a horizontal substrate. The mixing pattern shows that the fluid of the moving droplet is surrounded by the fluid of the stationary droplet. The moving droplet is deformed by the effect of the stationary droplet because the surface tension of the moving droplet is larger than that of the stationary droplet. The mixing pattern in the coalesced droplet is identical to the flow generated. Mixing is dominated both by convection as well as diffusion. Mushroom-shaped mixing pattern is observed inside the coalesced droplet.

Recirculation enhances convection dominated mixing as well as the rate of diffusion.

Coalescence of drops at the interface of two immiscible fluids was studied by Aryafar et al. (2006), Bach et al. (2004), Blanchette et al. (2009) and Bordoloi et al., (2012). Aryafar et al. (2006) studied drop coalescence at the interface of two immiscible fluids. Experimental results show a power law relation, $t \sim R^{3/2}$. The drop ratio is not constant and reduces when $Oh \to 0$. Effect of viscosity becomes comparable with inertia forces. The formation of a secondary drop does not follow inviscid theory. The viscosity ratio is important while examining the formation of a secondary drop. Bach et al. (2004) reported that small fluid dynamic stresses and deformation of the interface are produced when a drop approaches the interface. The drop deformation is proportional to the Weber number. A smaller daughter drop is produced when the mother drop coalesces with the interface. Weber number of the coalescing drops is lesser than unity which implies that the inertia of the mother drop is significant over surface tension. Blanchette et al. (2009) studied the coalescence of drops at the interface. Experiments show the existence of partial coalescence when the surface tension ratio is greater than 0.93. Viscous effects damp the capillary waves and decrease the spreading of low surface tension fluid. Size of the resulting drop during partial coalescence is directly proportional to surface tension ratio. Bordoloi et al. (2012) studied the coalescence of the drops at the interface. Rupture occurs off-axis near the rim of minimum film thickness. The initial axisymmetry is disturbed because of the perturbation of neighboring objects on one side of the drop. The film rupture is dominated by surface tension. Collapsing of the drop in the medium is governed by both gravity and an inward capillary contraction. A very rapid retraction of the ruptured interface as well as a fairly rapid collapse of the drop is because of smaller Ohnesorge number.

Impact of drop on a horizontal substrate was studied by Bayer et al. (2006) and Lagubeau et al. (2012). Bayer et al. (2006) reported that most of the impacts show an early presence of capillary waves. Increase in contact line velocity increases the contact angle of a wettable surface while contact angle of nonwettable surface is unaltered. Experimental results show power law relation for spreading diameter and impact velocity as $D_m / D_o \sim V_o^{2/7}$. Surface wettability strongly affects the contact line dynamics when Weber number is less than unity. Contact angle hysteresis on wettable and partially wettable surfaces decreases with reduced impact inertia.

Lagubeau et al. (2012) reported that spreading radius of the liquid patch increases with time. The central part of the liquid flattens with time and converges towards a constant film thickness while surface tension retracts the drop. A strong pressure field is experienced close to the impact region. The evolution of the drop can be modeled using a thin film approximation. The minimal film thickness scaling follows, $\delta \propto \mathrm{Re}^{-2/5}$ where δ is minimum film thickness. The transition time between the self similar regime and regime of minimal thickness, scales as, $t \propto \mathrm{Re}^{1/5}$ where t is transition time.

Most of the work on drop coalescence is reported for sessile drops while the present study is for coalescence of pendant drops. In light of the discussions given above, experiments have been performed to find shear stresses generated on the wall during coalescence of pendant drops. Water is used as a working fluid while the surface coating is Teflon.

2. EXPERIMENTS

Figure 1 shows the schematic drawing of an experimental set-up developed as a part of this work. It is used to image pendant drops on a horizontal surface. The pendant drop is imaged using a high speed camera from a direction normal to the vertical plane. A micro liter syringe with 100 µL capacity and a least count of 0.02 µL has been used to deposit pendant drops on the underside of the substrate.

Teflon was used as a substrate and contact angle for water was measured to be 90° in all the experiments reported here. Halogen light source as well as LED were used to illuminate the coalescing drops. A high speed camera (Photron fastcam SA-3)

was used for high speed imaging of the coalescing drops. Post processing of the images was carried out with programs written in MATLAB. Image processing programs have been developed to obtain center of mass of the coalesced drop, which in turn, yields velocity components. These velocity components are used to find the time-dependent shear stresses generated on the wall. Figure 2 shows the image sequence of coalescing drops as seen in the front-view for the drops of equal volume. Time evolution of drop shapes yields considerable change in properties in an image sequence. Similarly, Figure 3 shows the image sequence of coalescing drops as seen in the front-view for drops of unequal volumes. Figure 4 shows the image sequence of coalescing drops as seen in the side-view for drops of equal volumes. Time evolution of drop shapes does not show change in geometry in this image sequence. One can infer that the coalescence process can be analyzed based on the front-view alone. An image sequence in Figure 5 shows the repeatability of the experiments for coalescing drops of equal volumes as seen in the front-view.

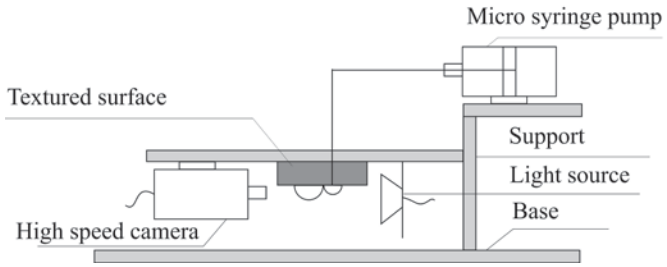

Figure 1: Schematic of experimental set-up

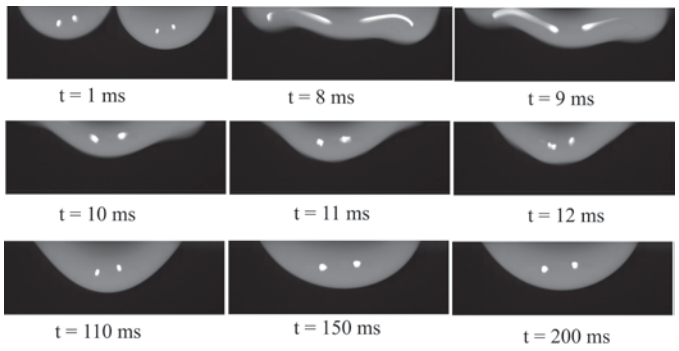

Figure 2: Image sequence of drop coalescence as seen in front-view for equal drops with d_1 = 1.01 mm and d_2 = 0.99 mm

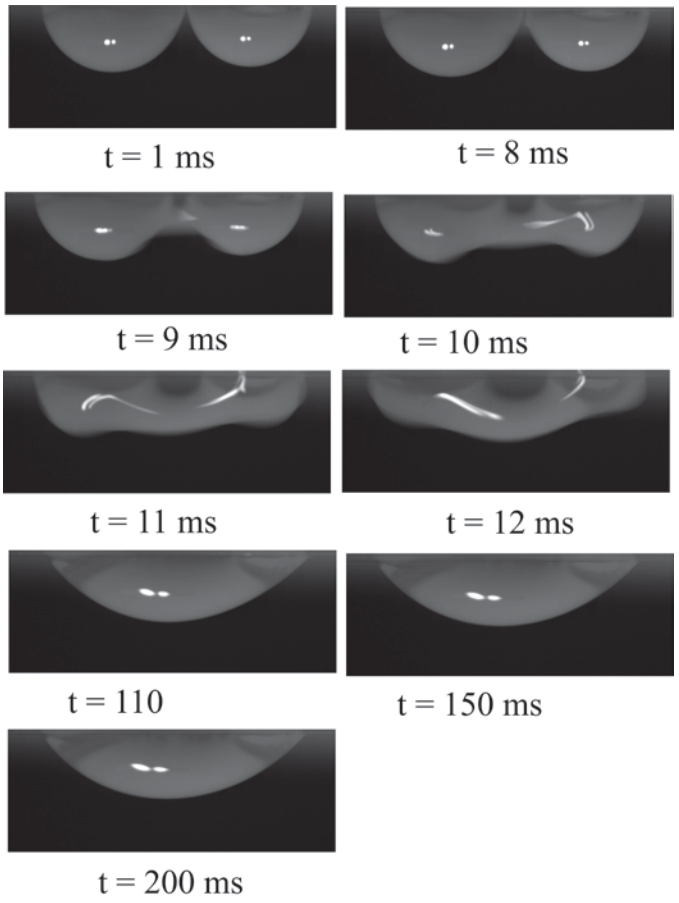

Figure 3: Image sequence of drop coalescence as seen in front-view for unequal drops with d_1 = 2.232 mm and d_2 = 1.898 mm

Experiments have been performed over a wide range of volumes. The characteristics length is defined as

$$L = (V_D)^{1/3} \tag{1}$$

The Bond number is defined as

$$Bo = \rho g L^2 / \sigma \tag{2}$$

The Ohnesorge number is defined as

$$Oh = \mu / \sqrt{\rho \sigma L} \tag{3}$$

$$\mathrm{Re} = \rho U L / \mu \tag{4}$$

Typical values of these dimensionless quantities are given in Table 1.

3. RESULTS AND DISCUSSIONS

Experiments are performed over a wide range of volumes and the results are plotted across various timescales. Coordinates of centroid are plotted as a function of time. The coordinates of the drop centroid in an image sequence yield velocity components. These velocity components are plotted with time. Further, these velocity components generate time dependent shear stresses on the wall.

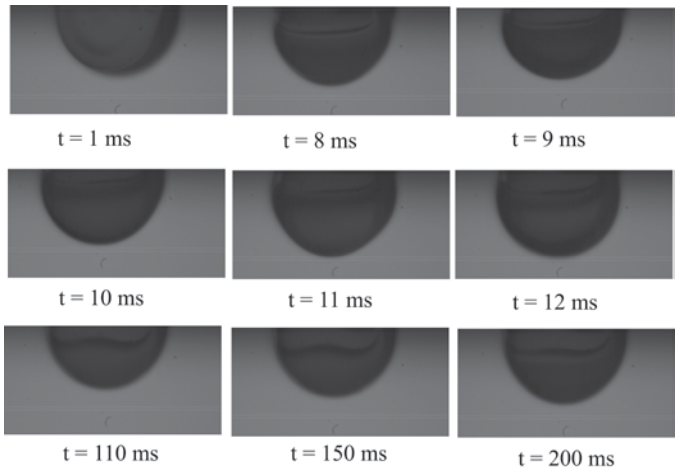

Figure 4: Image sequence of drop coalescence as seen in side-view for equal drops with d_1 = 3.13 mm and d_2 = 3.1 mm

Significance of the applicable forces is observed based on the non-dimensional numbers and their ability to unify data.

3.1 Calculations for Shear Rate

Shear rate is defined as the gradient of velocity in a flowing fluid.

x-component of the centroid is calculated from the image with N pixels as

$$x_c = \frac{\sum_{i=1}^{N} x_i \cdot \gamma_i}{\sum_{i=1}^{N} \gamma_i} \tag{5}$$

$\gamma_i = 1$ inside the drop and $\gamma_i = 0$ outside the drop

The *x*-components of centroid for a pair of images yield

$$u_c = \frac{(x_c)_{i+1} - (x_c)_i}{t_{i+1} - t_i} \tag{6}$$

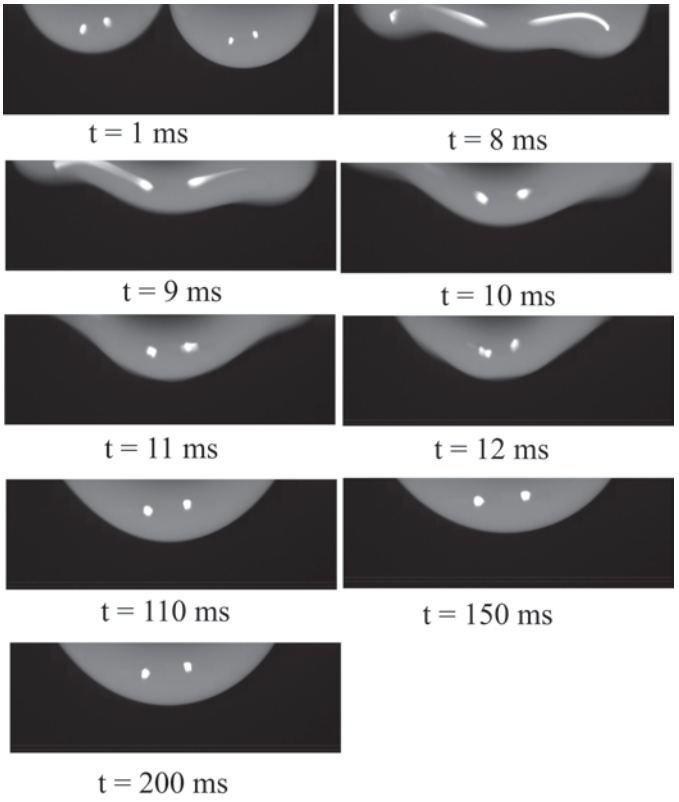

Figure 5: Image sequence of drop coalescence as seen in front-view for equal drops with d_1 = 2.2 mm and d_2 = 2.1 mm

Table 1: Range of non-dimensional numbers for a wide range of volumes in the experiments

Water (25°C and 1 atm.)	
d = 0.5 - 3 mm	
L = 0.4 – 2.4 mm	Bo = 0.022 – 0.783
	Oh = 0.0053 – 0.002
U = 0.063 – 0.153 m/s (based on gravity), Equation 11	U = 0.173 – 0.425 m/s (based on surface tension), Equation 14
Re = 25.074 – 365.369	Re = 68.856 – 1014.915

Similiarly, *y*-component of the centroid is calculated as

$$y_c = \frac{\sum_{i=1}^{N} y_i \cdot \gamma_i}{\sum_{i=1}^{N} \gamma_i} \tag{7}$$

The *y*-component of centroid in an image sequence yields,

$$v_c = \frac{(y_c)_{i+1} - (y_c)_i}{t_{i+1} - t_i} \tag{8}$$

The *x*-component and the *y*-component of centroid velocity yield,

$$\text{Shear rate} = \left| \frac{\partial u_c}{\partial y_c} - \frac{\partial v_c}{\partial x_c} \right| \tag{9}$$

$$\text{Shear rate} \approx \frac{(u_c)_i}{(y_c)_i} \tag{10}$$

3.2 Data in Dimensional Form

Figure 6 shows the variation of the *x*-coordinate of the centroid of coalesced drop with time. Higher oscillations are observed for a drop of equal volume than the drops of unequal volume. In case of equal volumes, the maximum value of *x*-coordinate of the centroid is 4.15 mm at the instant of coalescence and it becomes stable at a value of 3.9 mm. For unequal volumes, the maximum value of *x*-coordinate of the centroid is 3.55 mm at the instant of coalescence and it becomes stable at a value of 3.5 mm.

Figure 7 shows the variation of the *y*-coordinate of centroid with time. In case of equal volumes, the maximum value of *y*-coordinate of the centroid is 0.71 mm at the instant of coalescence and it becomes stable at a value of 0.5 mm. For unequal volumes, the maximum value of *y*-coordinate of the centroid is 0.51 mm at the instant of coalescence and becomes stable at a value of 0.4 mm.

Figure 8 shows the variation of the *x*-component of centroid velocity with time. In case of equal volumes, the maximum value of the *x*-component of centroid velocity is 25 mm/s during coalescence and becomes zero over a period of time. For unequal volumes, the maximum value of the *x*-component of centroid velocity is 50 mm/s during coalescence and becoming zero over a period of time. For small times, velocity in excess of 50 mm/s is realized.

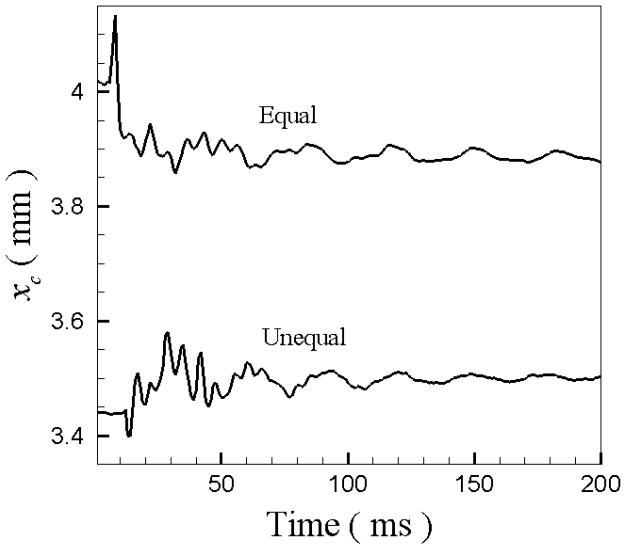

Figure 6: Variation of *x*-coordinate of centroid with time for equal and unequal drop volumes

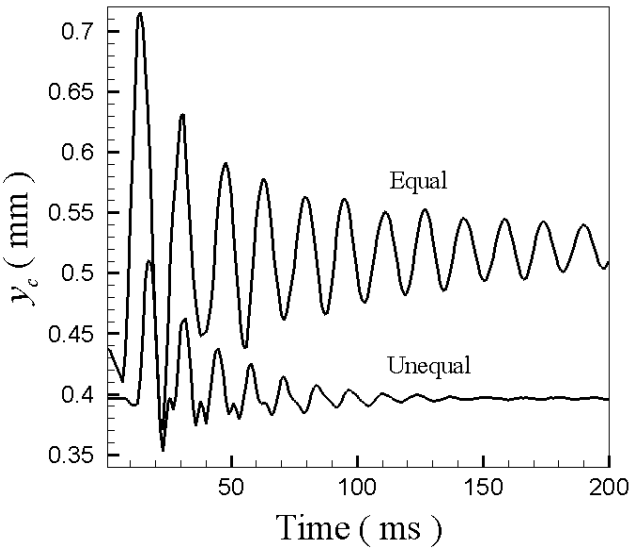

Figure 7: Variation of *y*-coordinate of centroid with time for equal and unequal drop volumes

Figure 9 shows the variation of *y*-component of centroid velocity with time. In case of equal volumes, the maximum value of centroid velocity along *y*-coordinate is 50 mm/s during coalescence becoming zero within around 200 ms. For unequal volumes, the maximum value of centroid velocity along the *y*-coordinate is 25 mm/s at the instant of coalescence becoming zero within around 100 ms. For small times, velocity in excess of 25 mm/s is realized.

Figure 10 shows the variation of shear rate with time. In case of equal volumes, the maximum value of shear rate is 40 s^{-1} during coalescence and becoming zero within 60 ms. For unequal volumes, the maximum value of shear rate is 100 s^{-1} during coalescence becoming zero within around 100 ms. For small times, shear rate in excess of 80 s^{-1} is realized.

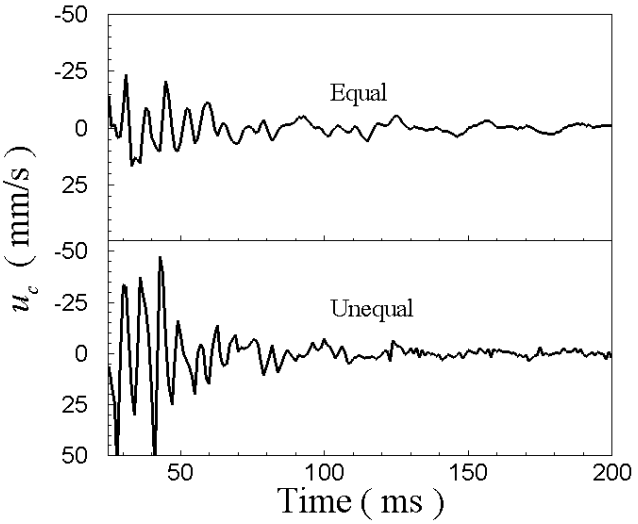

Figure 8: Variation of centroid velocity along *x*-coordinate with time for equal and unequal drop volumes

3.3 Non-dimensional Scaling Based on Gravity

Table 1 presents the non-dimensional numbers relevant to the present study. The value of Ohnesorge number indicates that the viscous forces are of secondary importance, though ultimately the fluid motion is stabilized by viscous dissipation. The value of Bond number indicates that the gravitational forces could be significant. There is no external flow field. Ultimately, the significant forces are gravitational forces and surface tension forces. Considering the significance of gravitational forces, velocity is defined as

$$U = \sqrt{gL} \tag{11}$$

and other parameters are non-dimensionalized as

$$x_c^* = \frac{x_c}{L},\quad y_c^* = \frac{y_c}{L},\quad u_c^* = \frac{u_c}{U},\quad v_c^* = \frac{v_c}{U} \tag{12}$$

$$\tau = \frac{t \cdot L}{U},\qquad \text{Shear rate}^* = \frac{\text{Shear rate} \cdot U}{L} \tag{13}$$

The length scale is given by Equation 1. Under gravitational scaling, the *y*-displacement of the centroid and *v*-component velocity gain prominence.

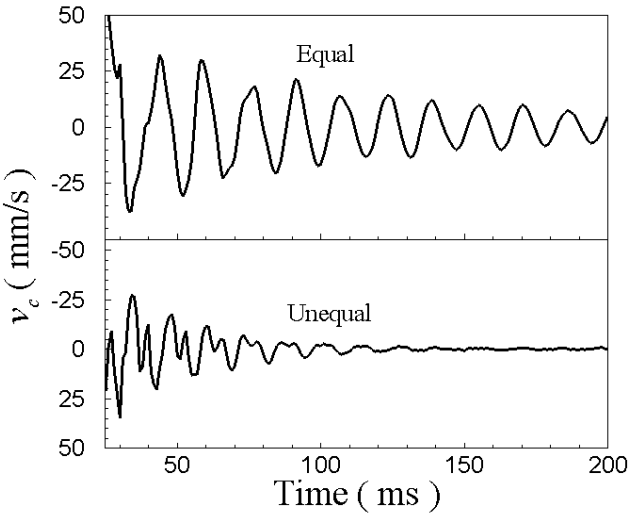

Figure 9: Variation of centroid velocity along *y*-coordinate with time for equal and unequal drop volumes

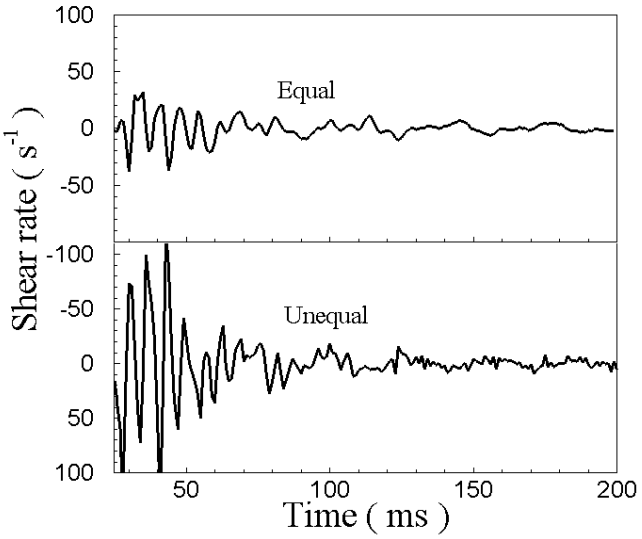

Figure 10: Variation of shear rate with time for equal and unequal drop volumes

Figure 11 shows the variation of non-dimensional *x*-coordinate of centroid with non-dimensional time. In case of equal volumes, the maximum value of non-dimensional *x*-coordinate of

centroid is 2.39 at the instant of coalescence and it remains constant at a value of 2.25 after dimensionless time of around 5. For unequal volumes, the maximum value of non-dimensional *x*-coordinate of centroid is 2.14 at the instant of coalescence and it remains constant at a value of 2.08 after dimensionless time of around 5.

Figure 12 shows the variation of non-dimensional *y*-coordinate of centroid with non-dimensional time. In case of equal volumes, the maximum value of non-dimensional *y*-coordinate of centroid is 0.41 at the instant of coalescence and it remains constant at a value of 0.3 after a dimensionless time of around 15. For unequal volumes, the maximum value of non-dimensional *y*-coordinate of centroid is 0.3 at the instant of coalescence and it remains constant at a value of 0.24 after a dimensionless time of around 7.

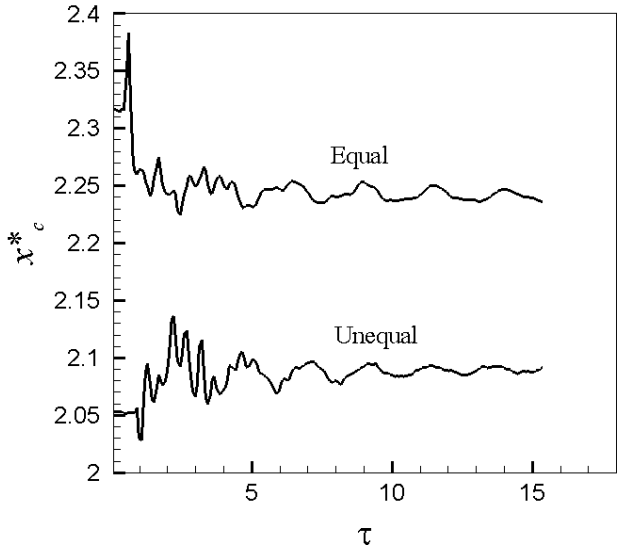

Figure 11: Variation of non-dimensional *x*-coordinate of centroid with non-dimensional time for equal and unequal drop volumes (for equal volumes, *Re* = 71; for unequal volumes, *Re* = 218)

Figure 13 shows the variation of non-dimensional centroid velocity along *x*-coordinate with non-dimensional time. In case of equal volumes, the maximum value of non-dimensional centroid velocity along the *x*-coordinate is 0.2 during coalescence becoming zero within a dimensionless time of around 7. For unequal volumes, the maximum value of non-dimensional velocity of centroid along *x*-coordinate is 0.4 during coalescence becoming zero within a dimensionless time of 6. For small non-dimensional times, non-dimensional velocity in excess of 0.5 is realized.

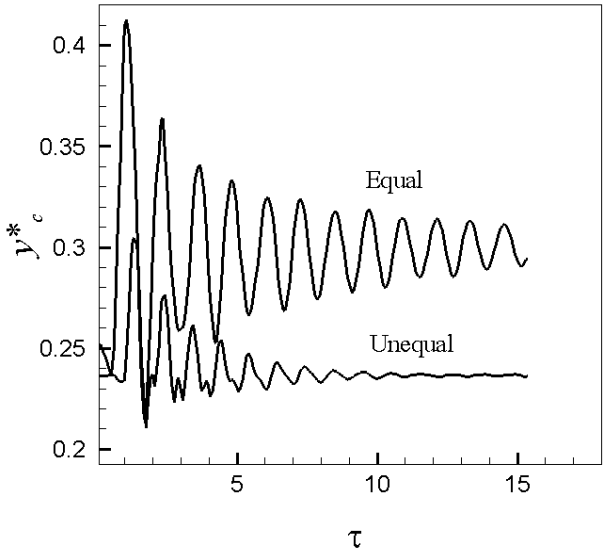

Figure 12: Variation of non-dimensional *y*-coordinate of centroid with non-dimensional time for equal and unequal drop volumes (for equal volumes, *Re* = 71; for unequal volumes, *Re* = 218)

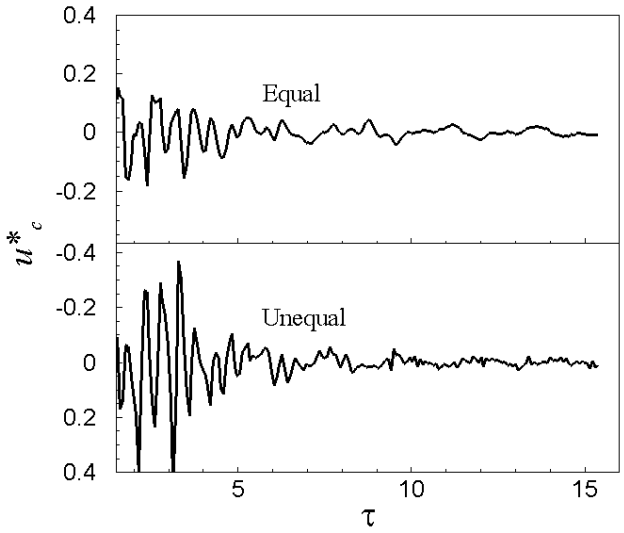

Figure 13: Variation of non-dimensional centroid velocity along *x*-coordinate with non-dimensional time for equal and unequal drop volumes (for equal volumes, *Re* = 71; for unequal volumes, *Re* = 218)

Figure 14 shows the variation of non-dimensional centroid velocity along *y*-coordinate with non-dimensional time. In case of equal volumes, the maximum value of non-dimensional centroid velocity along the *y*-coordinate is 0.4

during coalescence becoming zero within a dimensionless time of 6. For unequal volumes, the maximum value of non-dimensional velocity of centroid along *y*-coordinate is 0.35 during coalescence becoming zero over a period of time. For small non-dimensional times, non-dimensional velocity in excess of 0.1 is realized.

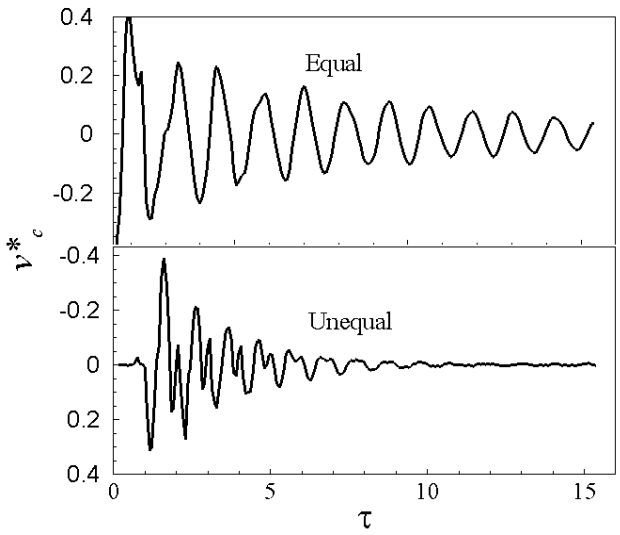

Figure 14: Variation of non-dimensional centroid velocity along *y*-coordinate with non-dimensional time for equal and unequal drop volumes (for equal volumes, *Re* = 71; for unequal volumes, *Re* = 218)

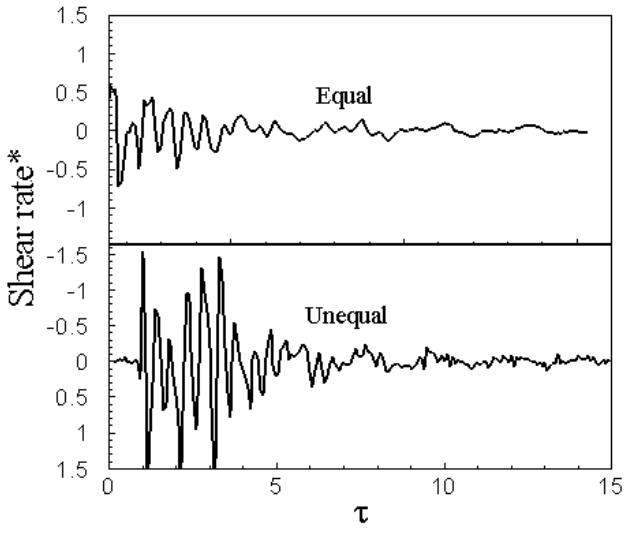

Figure 15: Variation of non-dimensional shear rate with non-dimensional time for equal and unequal drop volumes (for equal volumes, *Re* = 71; for unequal volumes, *Re* = 218)

Figure 15 shows the variation of non-dimensional shear rate with non-dimensional time. In case of equal volumes, the maximum value of non-dimensional shear rate is 0.5 during coalescence becoming zero within a dimensionless time of around 6. For unequal volumes, the maximum value of non-dimensional shear rate is 1.5 during coalescence becoming zero within a dimensionless time of around 6. For small non-dimensional times, non-dimensional shear rate in excess of 1.0 is realized.

3.4 Non-dimensional Scaling Based on Surface Tension

Considering the significance of surface tension forces, velocity is defined as

$$U = \sqrt{\frac{\sigma}{gL}} \tag{14}$$

and other parameters are non-dimensionalized as

$$x_c^* = \frac{x_c}{L},\quad y_c^* = \frac{y_c}{L},\quad u_c^* = \frac{u_c}{U},\quad v_c^* = \frac{v_c}{U} \tag{15}$$

$$\tau = \frac{t \cdot L}{U},\qquad \text{Shear rate}^* = \frac{\text{Shear rate} \cdot U}{L} \tag{16}$$

With surface tension getting prominence, the driver for fluid motion is pressure difference. Hence the *x*-displacement of the centroid and the *u*-component of the velocity are brought into prominence.

Figure 16 shows the variation of non-dimensional *x*-coordinate of centroid with non-dimensional time. In case of equal volumes, the maximum value of non-dimensional *x*-coordinate of centroid is 2.39 at the instant of coalescence and remains constant at a value of 2.25 after a dimensionless time of around 8. For unequal volumes, the maximum value of non-dimensional *x*-coordinate of centroid is 2.14 at the instant of coalescence and remains constant at a value of 2.08 after a dimensionless time of around 10.

Figure 17 shows the variation of non-dimensional *y*-coordinate of centroid with non-dimensional time. In case of equal volumes, the

maximum value of non-dimensional *y*-coordinate of centroid is 0.41 at the instant of coalescence and remains constant at a value of 0.3 after a dimensionless time of around 25. For unequal volumes, the maximum value of non-dimensional *y*-coordinate of centroid is 0.3 at the instant of coalescence and remains constant after a dimensionless time of around 13.

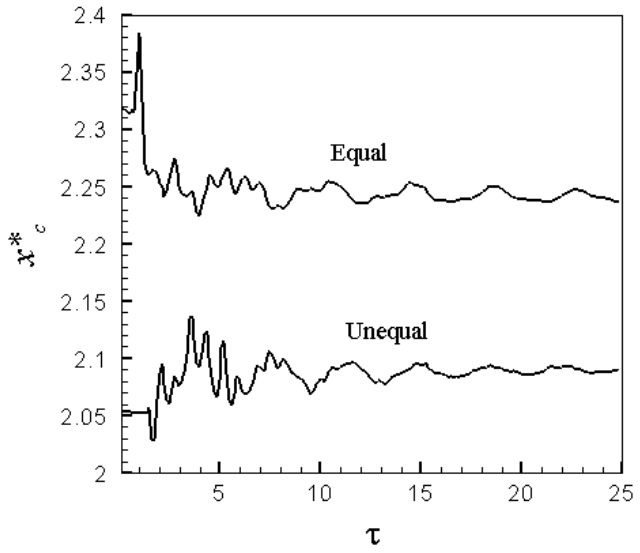

Figure 16: Variation of non-dimensional *x*-coordinate of centroid with non-dimensional time for equal and unequal drop volumes (for equal volumes, *Re* = 240; for unequal volumes, *Re* = 348)

Figure 18 shows the variation of non-dimensional centroid velocity along *x*-coordinate with non-dimensional time. In case of equal volumes, the maximum value of non-dimensional centroid velocity along *x*-coordinate is 0.15 during coalescence becoming zero within a dimensionless time of around 7. For unequal volumes, the maximum value of non-dimensional velocity of centroid along *x*-coordinate is 0.26 during coalescence becoming zero within a dimensionless time of around 9. For small non-dimensional times, non-dimensional velocity in excess of 0.35 is realized.

Figure 19 shows the variation of non-dimensional centroid velocity along *y*-coordinate with non-dimensional time. In case of equal volumes, the maximum value of non-dimensional centroid velocity along *y*-coordinate is 0.3 during coalescence becoming zero in a dimensionless time of around 25. For unequal volumes, the maximum value of non-dimensional velocity of centroid along *y*-coordinate is 0.26 during coalescence becoming zero within a dimensionless time of around 10. For small non-dimensional times, the non-dimensional velocity in excess of 0.1 is realized.

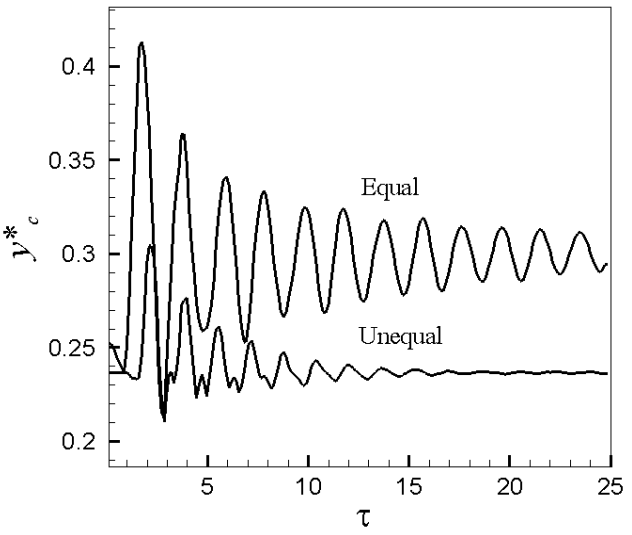

Figure 17: Variation of non-dimensional *y*-coordinate of centroid with non-dimensional time for equal and unequal drop volumes (for equal volumes, *Re* = 240; for unequal volumes, *Re* = 348)

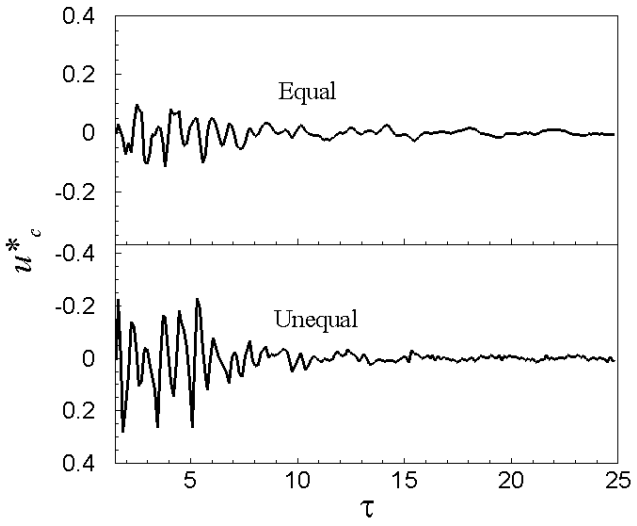

Figure 18: Variation of non-dimensional centroid velocity along *x*-coordinate with non-dimensional time for equal and unequal drop volumes (for equal volumes, *Re* = 240; for unequal volumes, *Re* = 348)

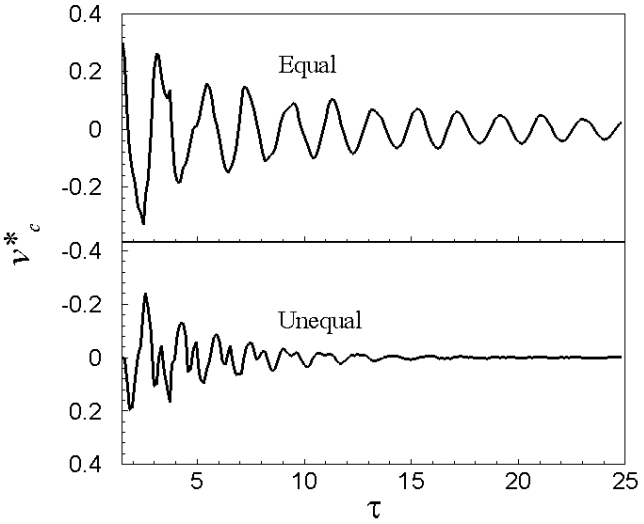

Figure 19: Variation of non-dimensional centroid velocity along *y*-coordinate with non-dimensional time for equal and unequal drop volumes (for equal volumes, *Re* = 240; for unequal volumes, *Re* = 348)

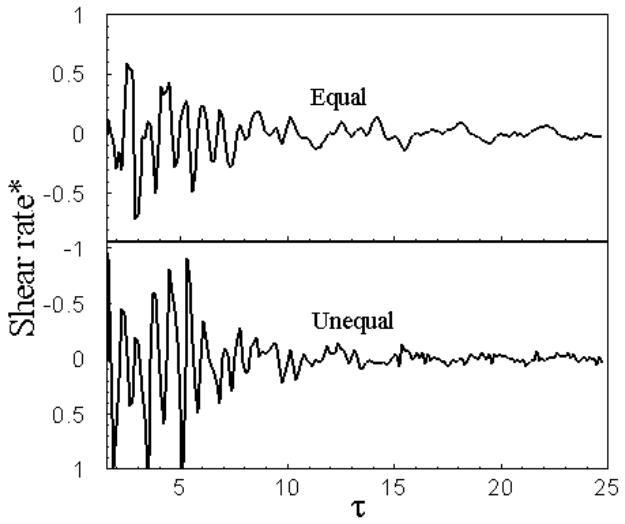

Figure 20: Variation of non-dimensional shear rate with non-dimensional time for equal and unequal drop volumes (for equal volumes, *Re* = 240; for unequal volumes, *Re* = 348)

Figure 20 shows the variation of non-dimensional shear rate with non-dimensional time. In case of equal volumes, the maximum value of non-dimensional shear rate is 0.5 during coalescence becoming zero within a dimensionless time of around 8. For unequal volumes, the maximum value of non-dimensional shear rate was 1.0 during coalescence becoming zero within a dimensionless time of around 10. For small non dimensional times, the shear rate in excess of 1.0 is realized.

3.5 Length and timescales

The coalescence process will generate its own length and timescales that are representative of the driving forces. One can expect gravity to be relevant to the vertical length scale and surface tension for the horizontal since the drops move towards each other by an internal pressure difference. In addition, appropriate timescales and Reynolds numbers can be defined. The timescales will depend on the energy released in the gravity field and change in surface energy due to the creation of a new surface relative to viscous dissipation. Length scales and timescales are found based on experimental observations. Denoted parent drops by 1 and 2 and the child drop as 3, the following definitions can be written.

Length scale based on gravity is given by

$$L_g = \frac{\left(m_1 g(y_c)_1 + m_2 g(y_c)_2\right) - \left((m_1 + m_2) g(y_c)_3\right)}{(m_1 + m_2) g} \quad (17)$$

Length scale based on surface tension is given by

$$L_\sigma = \left(\frac{V_1 (x_c)_1 + V_2 (x_c)_2}{V_1 + V_2} - (x_c)_3 \right) \quad (18)$$

The kinetic energy terms is expressed as $u_{rms}(t)$ and calculated as

$$u_{rms}(t) = \sqrt{\left(u_c^2(t) + v_c^2(t)\right)} \quad (19)$$

and the velocity scale $\tilde{u}$ is

$$\tilde{u} = \frac{u_{rms}^{\max} + u_{rms}^{\min}}{2} \quad (20)$$

The respective timescales and Reynolds numbers are

$$\tau_g = \frac{t^* \cdot \tilde{u}}{L_g} \qquad \tau_\sigma = \frac{t^* \cdot \tilde{u}}{L_\sigma} \quad (21)$$

$$\mathrm{Re}_g = \frac{\rho \cdot \tilde{u} \cdot Lg}{\mu} \qquad \mathrm{Re}_\sigma = \frac{\rho \cdot \tilde{u} \cdot Lg}{\mu} \qquad (22)$$

The timescale of coalescence (t^*) is the time required for the rms velocity to reduce to 1% of its peak value. The dimensionless quantities defined above are presented in Table 2.

Table 2: Length scales, timescales and Reynolds numbers for coalescence of water drops at 25°C and 1 atm. d_1 = 1.01 mm and d_2 = 0.99 mm.

L_g (mm) (Re_g)	0.0821(4.63)
L_σ (mm) (Re_σ)	0.82 (46.3)
$u_{rms}^{\max}$ (mm/s); [τ_g ; τ_σ]	113.6 [69.7; 6.9]
$\tilde{u}$ (mm/s)	56.8

Table 2 shows that the non-dimensional gravitational timescale is larger than that for surface tension while the length scales are reversed. One can conclude that the oscillations produced along the *y*-coordinate are smaller but persist for a longer time in comparison to those in the *x*-direction.

4. CONCLUSIONS

Water drops deposited on the underside of a Teflon substrate were imaged and analyzed in terms of the coordinates of the centroid during a coalescence process. The following conclusions have been arrived at in the present work.

1. The time dependent shear stress generated on the wall is momentary but the quantity is considerable enough to cause leaching of the surface coating.

2. Shear rate oscillations produced in the coalescing drops of unequal volumes are higher than for drops of equal volume.

3. Since large velocities are generated, local heat transfer coefficient is expected to be enhanced.

4. Oscillations generated along the *y*-coordinate take more time for settling down than those generated along the *x*-coordinate. These trends are well revealed in terms of the length and timescales defined on the basis of the relevant forces.

ACKNOWLEDGEMENTS

We thank the Board of Research for Nuclear Sciences, Mumbai for partial financial support.

REFERENCES

1. Andrieu, C., Beysens, D. A., Nikolayev, V. S., Pomeau, Y., 2002. Coalescence of sessile drops, J. Fluid Mech. 453 427.

2. Aryafar, H., Kavehpour, H. P., 2006. Drop coalescence through planar surfaces, Phys. Fluids 18 072105.

3. Bach, Gloria A., Koch, Donald L., GopinathArvind, 2004. Coalescence and bouncing of small aerosol droplets, J. Fluid Mech. 518 157–185.

4. Bayer, Ilker S., Megaridis, Constantine M., 2006. Contact angle dynamics in droplets impacting on flat surfaces with different wetting characteristics, J. Fluid Mech. 558 415–449.

5. Blanchette, François, Messio, Laura, Bush, John W. M., 2009. The influence of surface tension gradients on drop coalescence, Phys. Fluids 21 072107.

6. Bordoloi, Ankur Deep, Longmire, Ellen K., 2012. Effect of neighboring perturbations on drop coalescence at an interface, Phys. Fluids 24 062106.

7. Lagubeau, Guillaume, Fontelos, Marco A., Josserand, Christophe, Maurel, Agnès, Pagneux, Vincent, Petitjeans, Philippe, 2012. Spreading dynamics of drop impacts, J. Fluid Mech. 713 50-60.

8. Narhe, R., Beysens, D., Nikolayev, V. S., 2004. Contact line dynamics in drop coalescence and spreading,Langmuir 201213-1221.

9. Thoroddsen, S. T.,Takehara, K., Etoh, T. G., 2005[a]. The coalescence speed of a pendent and a sessile drop, J. Fluid Mech. 527 85–114.

10. Thoroddsen, S. T., Etoh, T. G., Takehara, K., Ootsuka, N., 2005[b]. On the coalescence speed of bubbles, Phys. Fluids 17 071703.

11. Thoroddsen, S. T., Qian, B., Etoh, T. G.,Takehara,K., 2007. The initial coalescence of miscible drops, Phys. Fluids 19 072110.

12. Wu, Mingming, Cubaud, Thomas, Ho Chih-Ming, 2004. Scaling law in liquid drop coalescence driven by surface tension, Phys. Fluids 16 L51.

13. Yeh, Szu-I, Fang, Wei-Feng, Sheen, Horn-Jiunn, Yang, Jing-Tang, 2013. Droplets coalescence and mixing with identical and distinct surface tension on a wettability gradient surface, Microfluidics and Nanofluidics 14 785–795.

NOMENCLATURE

Bo Bond Number = $\rho g L^2 / \sigma$

d_1 Diameter of bigger drop (m)

d_2 Diameter of smaller drop (m)

$\bar{g}$ Acceleration due to gravity (m/s^2)

L Characteristic dimension (m)

L_g Length scale based on gravity (m)

L_σ Length scale based on surface tension (m)

m Mass of drop (kg)

N Number of pixels

Oh Ohnesorge number = $\mu / \sqrt{\rho \sigma L}$

Re Reynolds number = $\rho U L / \mu$

t Time (s)

t^* Time constant (s)

U Characteristic velocity (m/s)

$\tilde{u}$ Mean root mean square velocity (m/s)

u_c *x*-component of centroid velocity (m/s)

$u_c(t)$ Instantaneous *x*-component of centroid velocity (m/s)

u_{rms} Root mean square velocity (m/s)

V Volume of drop (m^3)

v_c *y*-component of centroid velocity (m/s)

$v_c(t)$ Instantaneous *y*-component of centroid velocity (m/s)

V_D Volume of composite drop (m^3)

x_c *x*-coordinate of centroid (m)

y_c *y*-coordinate of centroid (m)

Greek symbols

γ Area function

μ Dynamic viscosity of fluid (Pa.s)

ρ Density of fluid (kg/m^3)

σ Surface tension (N/m)

τ Non-dimensional time